Science Press

Molten Pool Flow Morphology During Vacuum Arc Remelting Process for GH4698 Alloy

Zan Lei[1],　Luo Dehan[1],　Li Ying[1],　Zhang Jian[2],　Yu Yaowei[1]

[1] State Key Laboratory of Advanced Special Steel, Shanghai Key Laboratory of Advanced Ferrometallurgy, School of Materials Science and Engineering, Shanghai University, Shanghai 200444, China；[2] Chengdu Advanced Metal Materials Industry Technology Research Institute Co., Ltd,Chengdu 610000, China

Abstract: In order to further understand the vacuum arc remelting (VAR) process, with the help of OpenFOAM and an open source CFD computing software, a two-dimensional multi-physical finite volume model (FVM) including electromagnetic field, temperature field and flow field was established to study the macroscopic phenomenon of the unsteady solidification process for GH4698 nickel-based super alloy ingots. Results show that magnetic induction intensity induced by the current flowing from the crucible to the consumable electrode is mainly concentrated on the upper part of the ingot and rotates along the axis of the ingot. The magnetic induction intensity first increases and then decreases from the center to the edge of the ingot, and reaches the maximum value at the edge of the electrode. Thermal buoyancy and Lorentz forces are the main driving forces in the molten pool and their effect on the flow of molten pool is opposite.

Key words: vacuum arc furnace; finite volume model; electromagnetic field; flow field

---

Vacuum arc remelting (VAR) is a secondary melting process that consists of melting a consumable electrode by a direct current electric arc under vacuum condition to obtain homogeneous ingots for reactive and segregation sensitive alloys such as nickel-based superalloy which is widely used to produce aeroengine turbine disc. It has been found that an ingot with improved chemical homogeneity and reduced impurity content will be conducive to subsequent forging and engineering performance.

A schematic diagram of the VAR process is shown in Fig.1[1]. There is a vacuum environment in the VAR furnace. A cylindrical consumable electrode is loaded on the top of the water-cooled copper crucible. When the power is switched on, arcs are generated between the electrode and the initial material at the bottom of the crucible to melt each other. Molten alloy drops fall down from the electrode into the crucible, forming a molten pool. As cooling water takes away the heat from the molten pool in the crucible, liquid metal adjacent to the molten pool wall first solidifies, and then solidification happens gradually into the interior. Eventually a secondary ingot

Fig.1　Schematic of the vacuum arc remelting process [1]

---

forms in the crucible.

Numerical simulations of the VAR process have been developed progressively over the last 40 years for inferring the probable connection between the process parameters and the heat transfer and fluid flow. Compared with the experimental methods, the numerical simulation method is beneficial to reduce the research cost and shorten study time. Meanwhile, the post-processing software can be used to visually explore the nature of solidification and provide theoretical knowledge for ingot production.

In the early, the VAR simulation models only consider the heat transfer in the process[2], and then are developed to include fluid flow, electro-magnetic influences[3,4] and turbulence model[5]. After that, more transient models were proposed to study the molten pool in the axis direction of the ingot[6]. Then, the microstructure of ingot during VAR, has been simulated by coupling these macroscopic models with mesoscale or microscale models for making further investigation on the critical solidification mechanisms[7]. Recently, Pericleous et al[8] studied the growth of microstructure through simulation and explored the formation mechanism of freckle solidification defects. Patel et al[9] investigated the effect of different melting parameters (e.g., voltage) on the depth of molten ingot pool through the calculation software SOLAR. In addition, Spitans et al[10] studied the evolution of molten pool flow morphology during the growth of ingots under the action of magnetic field.

Although the past works have made some studies on electromagnetic and flow fields, the research on coupling of these macroscopic physical fields is very scarce. The microstructure properties of nickel-based superalloy ingots are largely dependent on the flow state in the molten pool. Lorentz force is one of the main driving forces of fluid movement in the molten pool. Therefore, it is of great significance to study in detail and understand the phenomenon of molten alloy flow in the molten pool.

In this research, a two-dimensional multi-physical field coupled finite volume model including electromagnetic field, temperature field and flow field of the VAR process was established to simulate the macroscopical heat and momentum transport during solidification. The solidification process and flow pattern of liquid alloy metal under multiple physical fields were discussed.

1 Model Theory

The chemical compositions (wt%) of GH4698 alloy are shown in Table 1[11]. And a 2D geometry of VAR furnace along a radius of crucible is shown in Fig.2. It consists of a cylindrical copper crucible, a pool of liquid metal, ingot and consumable electrode. A two-dimensional macroscopic model was established for simulating the above VAR process based on assumptions as follows.

(1) Molten alloy fluid belongs to incompressible Newtonian fluid and laminar flow.

(2) Thermophysical properties are approximated as constants in the molten alloy and ingot with the exception of

mush zone, in which thermophysical properties are set as liner function of liquid fraction.

(3) Surface arc pressure and metal steam pressure are both neglected.

(4) Chemical reactions in the molten pool and Marangoni flow are also neglected[12].

(5) Heat radiation is neglected on the surface of the VAR molten pool.

(6) Boussinesq approximation works for alloy density.

Because Reynolds number of liquid metal pool happen in the transition range, laminar flow hypothesized in this research is reasonable to use[13]. Another reason is that a three-dimensional turbulent model takes a lot of computational cost. Therefore a two-dimensional laminar model is chosen in the simulation.

Combining other statements given by assumptions (2)~ (6) with assumptions 1, all these assumptions slightly reduce the accuracy of the prediction of the pool temperature field but greatly improve the efficiency of the calculation and largely reduce computational time.

1.1 Electromagnetic field

Since fluid flow is much slower than current flow, the conservation equation of electric potential in steady state and the fluctuation equation of magnetic vector potential in static magnetic field are solved. Electric potential conservation equation and fluctuation equation of magnetic vector potential are given by

$$\nabla \cdot (-\sigma \nabla \phi) = 0 \qquad (1)$$

$$\nabla \cdot (\nabla A) = \sigma \mu \nabla \phi \qquad (2)$$

By solving the above two equations, the magnetic induction intensity and current density can be expressed:

$$B = \nabla \times A \qquad (3)$$

$$J = -\sigma \nabla \phi \qquad (4)$$

Table 1   Chemical composition of GH4698 alloy (wt%)[11]

Cr	C	Mo	Al	Ti	Nb	Ni
14.55	0.048	3.21	1.77	2.68	2.02	Bal.
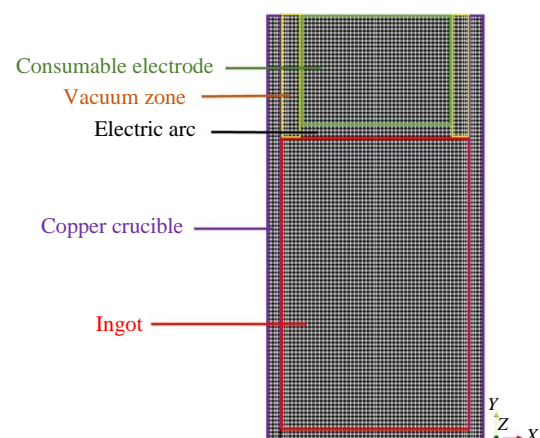
Fig.2 2D geometry of VAR furnace by hexahedral structured meshes

1.2 Flow and thermal field

By solving the Navier-Stokes equations and energy conservation equation in liquid melt pool and mushy zone of the ingot, the velocity field and temperature field changing with time are obtained.

These conservation equations can be expressed as follows.

(1) Continuity equation:

$$\nabla \cdot (\rho \boldsymbol{U}) = 0 \tag{5}$$

(2) Momentum equation:

$$\frac{\partial (\rho u)}{\partial t} + \nabla \cdot (\rho \boldsymbol{U} u) = \nabla \cdot (\rho \nabla u) - \frac{\partial P}{\partial x} + S_x \tag{6}$$

$$\frac{\partial (\rho v)}{\partial t} + \nabla \cdot (\rho \boldsymbol{U} v) = \nabla \cdot (\eta \nabla v) - \frac{\partial P}{\partial y} + S_y \tag{7}$$

where S_x and S_y are given by

$$S_x = -C \frac{(1 - \gamma)^2}{\gamma^3 + b} u + (\boldsymbol{J} \times \boldsymbol{B})_x \tag{8}$$

$$S_y = -C \frac{(1 - \gamma)^2}{\gamma^3 + b} v + (\boldsymbol{J} \times \boldsymbol{B})_y + \rho g [1 - \max (\beta (T - T_s))] \tag{9}$$

The first term of S_x and S_y in Eq.(6) and Eq.(7) represents the pressure change caused by the fluid flowing through the mush zone[14]. The second term is the component of Lorentz force in their respective direction. The last term of S_y is the thermal buoyancy assumed by Boussinesq approximation. Furthermore, γ is expressed as the error function of temperature[15]:

$$\gamma = 0.5 \text{erf} \left[\frac{4 (T - T_m)}{(T_1 - T_s)} \right] + 0.5 \tag{10}$$

(3) Energy equation:

$$\frac{\partial (\rho c T)}{\partial t} + \nabla \cdot (\rho \boldsymbol{U} c T) = \nabla \cdot (\lambda \nabla T) + S_h \tag{11}$$

The source term, S_h, accounts for the latent heat and Joule heat produced inside a unit volume per unit time:

$$S_h = -L \frac{\partial (\rho \gamma)}{\partial t} - L \nabla \cdot (\rho \boldsymbol{U} \gamma) + \frac{J^2}{\sigma} \tag{12}$$

where the first term of S_h is the latent heat released by the phase transition in the local region, and the second term defines the latent heat flux caused by the movement of the phase interface. The final term is the Joule heat generated by the current density. For the heat conduction of the crucible, it is expressed as Eq.(4).

(4) Laplace equation of temperature transfer:

$$\frac{\partial (\rho_{cru} c_{cru} T)}{\partial t} - \nabla \cdot (\lambda_{cru} \nabla T) = 0 \tag{13}$$

All of the mathematical symbols used above are defined as follows: specific heat capacity of crucible c_{cru} in J/(kg·K), velocity $\boldsymbol{U}$ in m/s, electric potential φ in V, temperature T in K, ingot thermal conductivity λ in W/(m·K), liquidus temperature T_1 in K, electrical conductivity σ in $\Omega^{-1} \cdot m^{-1}$, solidus temperature T_s in K, magnetic permeability μ in H/m, Arithmetic mean T_m between T_1 and T_s in K, volumetric thermal expansion coefficient β in K^{-1}, pressure P in Pa, liquid fraction γ, magnetic induction intensity $\boldsymbol{B}$ in T, Darcy dimensionless number b, current density $\boldsymbol{J}$ in A/m², error function erf in Eq.(10), magnetic vector potential A in T·m, latent heat of solidification L in J/kg, time t in s, density of crucible ρ_{cru} in kg/m³, Darcy constant C in kg/(m³·s), gravitational acceleration $\boldsymbol{g}$ in m/s², crucible thermal conductivity λ_{cru} in W/(m·K), maximum function max in Eq.(9), velocity u in x coordinate in m/s, specific heat capacity of ingot c in J/(kg·K), velocity v in y coordinate in m/s, density of ingot ρ in kg/m³, and dynamic viscosity η in Pa·s.

1.3 Boundary conditions and thermophysical properties

For the electromagnetic field, a positive potential is applied to the upper part of the crucible, and the upper part of the electrode is zero potential. There is no magnetic flux leakage outside the model, so parallel boundary condition of magnetic vector potential is applied in the calculation area.

For the solution of momentum conservation equation, no slip boundary condition is applied to the interface between the ingot and crucible and the upper part of the ingot.

The initial condition of the energy conservation equation is temperature value of overheating. Temperature of cooling water is considered as the boundary condition of the external wall of the crucible. A mixed boundary condition is used for coupling the temperature at the interface and both sides of the interface use a mix of zero gradient and neighbor value. For pressure and liquid fraction field, boundary condition are both zero gradient.

These default simulation conditions and thermophysical properties used are listed in Table 2.

1.4 Numerical simulation procedure

This numerical simulation work takes pimple algorithm to be a basic framework and the specific algorithm is described as follows.

(1) The potential distribution and the magnetic vector potential distribution are predicted by explicitly solving the po-

Table 2 Default simulation conditions and thermophysical properties

Property	Value
Ingot diameter/m	0.508
Crucible outer diameter/m	0.548
Electrode diameter/m	0.44
Volts/V	21
Density of ingot/kg·m⁻³	7471
Density of crucible/kg·m⁻³	8940
Liquidus temperature/K	1637.15
Solidus temperature/K	1488.15
Expansion coefficient/K⁻¹	1.8×10⁻⁵
Latent heat/J·kg⁻¹	2.72×10⁵
Specific heat capacity of ingot/J·(kg·K)⁻¹	620
Specific heat capacity of crucible/J·(kg·K)⁻¹	383
Thermal conductivity of crucible/ W·(m·K)⁻¹	390
Dynamic viscosity/Pa·s	5.0×10⁻³
Electric conductivity of ingot/Ω⁻¹·m⁻¹	1.0×10⁶
Electric conductivity of crucible/Ω⁻¹·m⁻¹	5.0×10⁷
Magnetic permeability/H·m⁻¹	1.26×10⁻⁶

tential conservation equation and the magnetic vector potential wave equation. Then the current density and magnetic induction intensity are obtained. After that the initial value of Lorentz force is obtained by cross product, and is substituted into the momentum conservation equation as a volume force.

(2) The momentum equation is solved by the initial conditions and boundary conditions. The pressure gradient term is calculated by the pressure distribution from the previous iteration or an initial guess. The momentum equation is under-relaxed in a semi-implicit manner and is called the momentum predictor. The solution of the momentum equation gives an approximation of a new velocity field.

(3) Magnetic flux term on cell faces is evaluated to solve Poisson equation for electric potential. Then current density flux is calculated by normal gradient of electric potential on cell faces and magnetic flux. The value at the center of the face is considered later by reconstruction employing consistent scheme: a volume weighted interpolation between cell face center and centroid. The final conservative current density distribution is employed to calculate the Lorentz force.

(4) The pressure Poisson equation is formulated and solved in order to obtain the new pressure distribution. In this step, a new set of conservative fluxes is calculated. The new pressure field includes both the pressure error and convection-diffusion error. In order to predict a better approximation of the correct pressure field, it will be necessary to solve the pressure Poisson equation many times. In addition, the non-linear effects are more important than the case of transient calculations. It is enough to obtain an approximation of the pressure field and recalculate the velocity matrix coefficients with the new set of conservative fluxes. The pressure solution is then under-relaxed in order to take into account the velocity part of the error. Then the velocity correction is done in an explicit manner by the new pressure distribution. This is the explicit velocity correction stage. Finally, continuity equation is solved to estimate errors and boundary conditions for velocity are updated.

(5) The conservative velocity flux is substituted into the energy conservation equation to predict the temperature field. Then the liquid fraction is updated by error function. Finally the relevant thermophysical parameters are calculated by linear calculation of the liquid fraction.

(6) Convergence criterions are monitored for all equations. If the system is not converged, a new iteration starts from Step (2). If all the equations converge, the calculation moves to the next time step.

2 Results and Discussion

2.1 Residual error curves in simulation

According to Fig.3, it is obvious that the residuals errors of temperature, velocity and pressure decrease with the increase of calculation time, and it is generally considered that the residual error of this order of magnitude has reached the requirement of convergence (10^{-5} for temperature, 10^{-5} for velocity, and 10^{-6} for pressure).
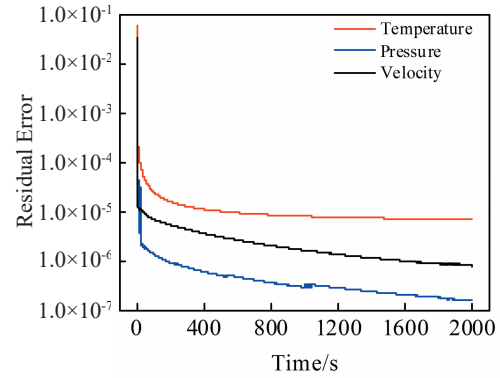
Fig.3   Residual error curves of simulation in VAR process

2.2 Distribution of electromagnetic field

In Fig.4, remelting current is mainly concentrated on the upper part of the crucible wall, the surface of the molten pool and the electrode. There is a short path among the current which flows from the crucible to the electrode and almost no current at the bottom of the ingot and crucible.

Fig.5 shows the current density distribution in all directions on the surface of the molten pool. When the current flows from the crucible wall to the electrode, current density becomes strong gradually, reaches the maximum value at the intersection of the ingot and the electrode edge and then decreases at the center (blue curve). The current density in the X direction decreases to zero at the center of the ingot (red curve). It has symmetrical distribution in the Y direction (green curve).

The distribution of magnetic field induced by remelting current is shown in Fig.6. Magnetic field is symmetrical about the axis of the ingot, which is consistent with Ref.[16]. Furthermore, its direction is decided by right hand law. Fig. 7 shows the magnetic flux of the molten pool surface from the axis to the edge of ingot. The magnetic density increases firstly and then decreases from the axis to the edge of ingot and
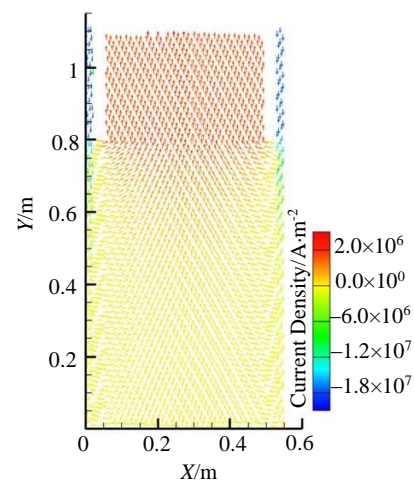
Fig.4   Distribution of remelting current in the crucible
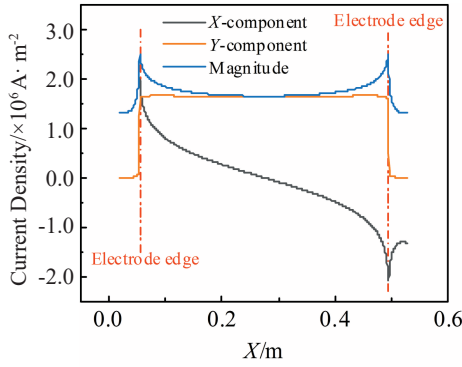
Fig.5   Current density on the surface of the molten pool
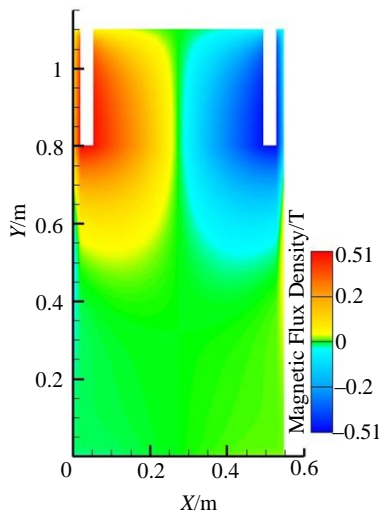
Fig.6   Distribution of magnetic field in ingot
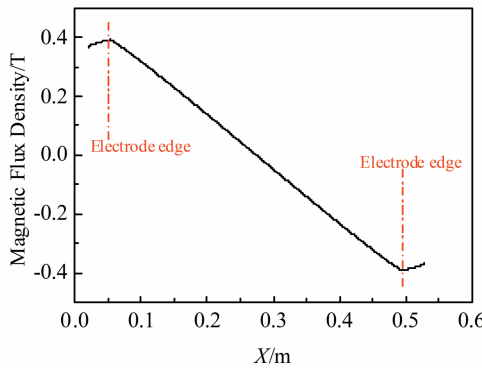
Fig.7   Magnetic flux of the molten pool surface

gets a maximum value at the electrode edge according to Ampere's law.

2.3 Evolution of solidification process

According to the calculation results, 100 and 1300 s were

randomly selected to present the temperature field and liquid phase fraction field.

Fig. 8 and Fig. 9 show that the heat in the molten pool is continuously extracted by the outer wall of the crucible, which forces the liquid metal in the crucible to solidify gradually along the direction of the vertical crucible. The isoline of the liquid fraction=0.5 gradually moves to the interior of the model as the calculation time extends, and the solidification part of the liquid metal gradually increases in Fig.10.

In order to compare the distribution of the flow field in the molten pool, the same geometry with and without electromagnetic field was calculated, and the results at the same time are shown in Fig.11 and Fig.12.

When no electromagnetic field is applied to the molten pool in Fig. 11, thermal buoyancy generated by temperature gradient in the molten pool drives the liquid metal to sweep the surface of the molten pool radially outward, and then
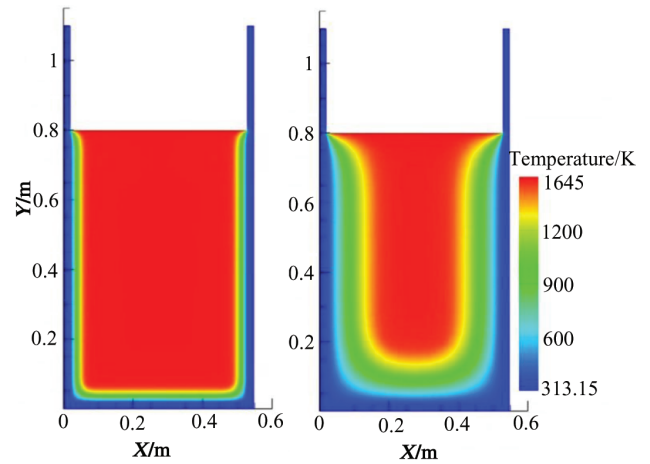
Fig.8   Dynamic variation of temperature field in ingot and crucible：
（a）t=100 s and（b）t=1300 s
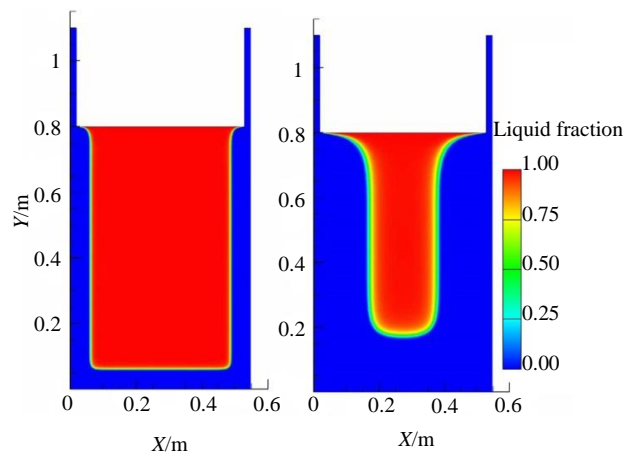
Fig.9   Dynamic variation of liquid fraction field in ingot：（a）t=
100 s and（b）t=1300 s
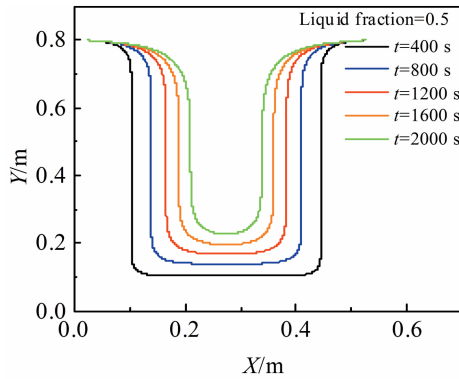
Fig.10   Dynamic variation of liquid fraction（0.5）with time
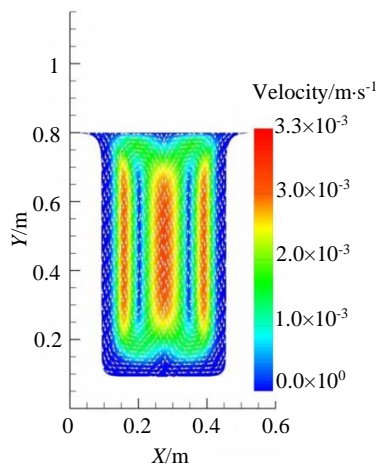
Fig.11   Flow field resulting from buoyancy at 300 s
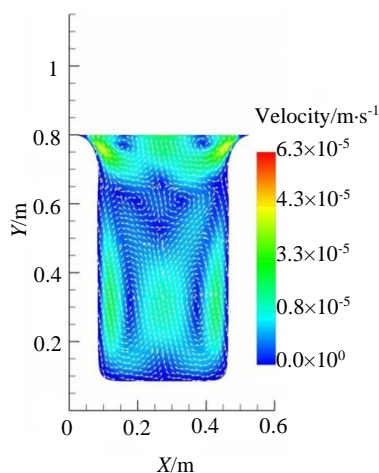
Fig.12   Flow field resulting from buoyancy and Lorentz force at 300 s

returns to the central axis of the molten pool along the bottom of the molten pool. Therefore, a clockwise flow forms on the right side of the axis.

After an electromagnetic field is applied to the molten pool in Fig.12, Lorentz force will have an effect on the flow of the fluid contrary to the thermal buoyancy. Therefore, the flow in counterclockwise direction appears in the upper part of the right axis of the molten pool. This flow pattern is consistent with the calculation results obtained by other researchers in similar VAR simulation[17].

Comparing Fig. 11 with Fig. 12, we can know that the electromagnetic force has an effect on reducing velocity magnitude velocity of liquid alloy pool.

3 Conclusions

1) Remelting current is mainly concentrated on the upper part of the crucible wall, the surface of the molten pool and the electrode, and there is almost no current at the bottom of the ingot and crucible. Current density reaches the maximum value at the intersection of the ingot and the electrode edge on the surface of the molten pool.

2) The magnetic field is symmetrical about the axis of the ingot. The magnetic density increases firstly and then decreases from the axis to the ingot edge and gets the maximum value at the electrode edge.

3) The heat in the molten pool is continuously extracted by the outer wall of the crucible, which forces the liquid metal in the crucible to solidify gradually inward along the direction of the vertical crucible.

4) Lorentz force has an effect on the flow of the fluid contrary to the thermal buoyancy.

References

1   Patel A D, Minisandram R S, Evans D G. *Proceedings of 10th International Symposium on Superalloys*[C]. PA: National Aeronautics and Space Administration, 2004: 917

2   Ballantyne A, Mitchell A. *Ironmaking & Steelmaking*[J], 1977, 4(4): 222

3   Bertram L, Zanner F. *Proceedings of Modeling of Casting and Welding Processes*[C]. Runge: OSTY GOV, 1980

4   Bertram L, Zanner F. *Proceedings of IUTAM Symposium on Metallurgical Applications of MHD*[C]. Cambridge: OSTY GOV, 1982

5   Gartling D, Sackinger P. *International Journal for Numerical Methods in Fluid*[J], 1997,24(12): 1271

6   Jardy A, Falk L, Ablitzer D. *Ironmaking & Steelmaking*[J], 1992, 19(3): 226

7   Xu X, Zhang W, Atwood R *et al. Proceedings of the Int Symp on Liq Met Proc and Cast*[C]. Santa Fe: AVS, 1999: 76

8   Pericleous K, Djambazov G, Ward M *et al. Metallurgical and Materials Transactions A*[J], 2013, 44(12): 5365

9   Patel A, Tripp D W, Fiore D. *Proceedings of the 2013 International Symposium on Liquid Metal Processing & Casting*[C]. Texas: Springer, 2013: 241

10   Spitans S, Franz H, Scholz H *et al. Magnetohydrodynamics*[J], 2017, 53(3): 557

Zan Lei et al. / Rare Metal Materials and Engineering, 2021, 50(4):1125-1131

11 Zhang P, Hu C, Zhu Q *et al. Materials Design[*J], 2015, 65: 1153

12 Lee P, Lothian R, Hobbs L *et al. Proceedings of Superalloys* [C]. Pennsylvania: Minerals, Metals and Materials Society, 1996: 435

13 Xu X, Zhang W, Lee P. *Metallurgical and Materials Transactions A*[J], 2002, 33(6): 1805

14 Voller V R, Prakash C. *International Journal of Heat and Mass Transfer*[J], 1987, 30(8): 1709

15 Rösler F, Brüggemann D. *Heat and Mass Transfer*[J], 2011, 47 (8): 1027

16 Kou H, Zhang Y, Yang Z *et al. International Journal of Engineering & Technology*[J], 2012, 12(1): 50

17 Zanner F, Williamson R, Harrison R *et al. Proceedings of International Symposium on Alloy 718 Metallurgy and Applications* [C]. PA: OSTY GOV, 1989: 17

GH4698合金真空电弧重熔过程中熔池流动形态

昝 磊[1]，罗德焙[1]，李 映[1]，张 健[2]，于要伟[1]

(1. 上海大学 材料科学与工程学院 省部共建高品质特殊钢冶金与制备国家重点实验室，上海 200444)
(2. 成都先进金属材料产业技术研究院有限公司，四川 成都 610000)

摘 要：为了进一步了解真空电弧重熔（VAR）过程，利用开源CFD计算软件OpenFOAM，基于有限体积法（FVM）建立了包括电磁场、温度场和流场的二维多场耦合模型来研究宏观非稳态下GH4698镍基合金铸锭的凝固过程。结果表明，从坩埚流向自耗电极的电流所引发的磁场主要集中在铸锭的上部，并沿铸锭轴线旋转。磁感应强度由铸锭中心向边缘呈现先增大后减小的趋势，并在电极边缘处达到最大值。热浮力和洛伦兹力是熔池内的主要驱动力，并且它们对熔池流动的影响正好相反。

关键词：真空电弧炉；有限体积模型；电磁场；流场

作者简介：昝 磊，男，1993年生，硕士，上海大学省部共建高品质特殊钢冶金与制备国家重点实验室，上海 200444，电话：021-96928188，E-mail: zanlei@shu.edu.cn